Article

Nanocrystals Modified with Peptide Nucleic Acids (PNAs) for Selective Self-Assembly and DNA Detection

Raj Chakrabarti, and Alexander M. Klibanov

J. Am. Chem. Soc., **2003**, 125 (41), 12531-12540• DOI: 10.1021/ja035399g • Publication Date (Web): 18 September 2003

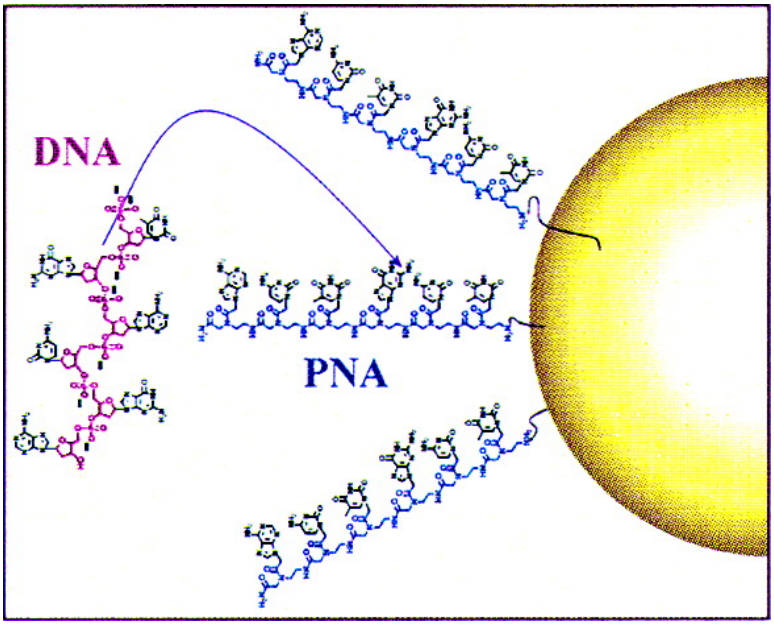

More About This Article

Additional resources and features associated with this article are available within the HTML version:

- Supporting Information
- Links to the 6 articles that cite this article, as of the time of this article download
- Access to high resolution figures
- Links to articles and content related to this article
- Copyright permission to reproduce figures and/or text from this article

View the Full Text HTML

J|A|C|S
ARTICLES
Published on Web 09/18/2003

Nanocrystals Modified with Peptide Nucleic Acids (PNAs) for Selective Self-Assembly and DNA Detection

Raj Chakrabarti and Alexander M. Klibanov*

Contribution from the Department of Chemistry and Division of Biological Engineering, Massachusetts Institute of Technology, 77 Massachusetts Avenue, Cambridge, Massachusetts 02139

Received March 31, 2003; E-mail: klibanov@mit.edu

Abstract: Gold nanocrystals modified with peptide nucleic acids (PNAs) have been prepared and applied to self-assembly and DNA sensing. Experiments with different PNA structural motifs show that (1) the versatility in PNA synthetic design can be used to modulate the electrostatic surface properties of nanocrystals, presenting an opportunity to control assembly rate and aggregate size, (2) short (6 base) PNAs can hybridize effectively while attached to nanoparticles, providing a route to generating materials with small interparticle spacings, and (3) the superior base pair mismatch selectivity of PNAs is further enhanced on nanosurfaces, enabling PNA-modified nanoparticles to act as highly selective nanoscale sensors, as well as synthons for defect-free self-assembly. This last feature was coupled with a substantial change in colloidal stability upon DNA hybridization to develop a novel colorimetric DNA assay that detects the presence of single base imperfections within minutes. Various modes of PNA hybridization, including the first practical application of PNA−PNA interactions, were used to direct the assembly of nanoparticles into macroscopic arrangements. Shorter duplex interconnects and greater specificity in assembly were obtained compared to similar experiments with DNA-modified nanocrystals.

Introduction

DNA nanotechnology is some two decades old.[1] The same features that make DNA an effective molecule for the storage of genetic information also render it useful as an engineering material for the construction of objects at the nanometer scale because of its ability to self-organize into desired structures via the specific hybridization of complementary sequences. Recently, DNA-directed assembly of nanoparticles has demonstrated that programmed assembly of nanostructures into heterogeneous multicomponent solids is possible.[2,3] For such materials to have useful physical properties, however, they should satisfy three criteria. First, interparticle spacings should be small so that the optical and electronic properties of neighboring nanocrystals are strongly coupled.[4] Second, the fidelity of assembly should be high enough that particles encoded by similar sequences are directed only to their designated positions in the lattice. Third, the assemblies should be well-ordered, since spatial disorder can result in undesirable changes in collective physical phenomena.

Despite the appealing prospects of programmed nanoparticle assembly, its practical application has been hampered by inability to generate materials bearing these characteristics. To form stable duplexes, DNA strands must be considerably longer than the nonpolar ligands commonly used to assemble nanoparticles by van der Waals and solvophobic interactions, precluding the possibility of strong coupling.[4] Although Watson−Crick base pairing is remarkably specific, the mismatch discrimination of DNA duplexes is not sufficiently selective to avoid the defective assembly of particles tagged with sequences differing in one or a few bases.[5] Finally, DNA-directed nanoparticle assemblies are not crystalline like those generated using nonpolar ligands. The high negative charge density of DNA may constrain the range of the interaction potential to a regime that is unsuitable for crystallization. Underscoring the importance of electrostatic interactions in assembly, the melting behavior of DNA-assembled nanoparticle aggregates has recently been shown to be very sensitive to the surface charge on the particles.[6]

In this study, we examined the use of peptide nucleic acids (PNAs), DNA analogues in which the entire sugar−phosphate backbone is replaced by a polyamide backbone, as a means of overcoming these obstacles. PNA complexes[7] offer two distinct advantages for nanomaterials synthesis: (1) greater stability than

(1) Seeman, N. C. *Nano Lett.* **2001**, *1*, 22−25.
(2) Mirkin, C. A.; Letsinger, R. L.; Mucic, R. C.; Storhoff, J. J. *Nature* **1996**, *382*, 607−609.
(3) Mitchell, G. P.; Mirkin, C. A.; Letsinger, R. L. *J. Am. Chem. Soc.* **1999**, *121*, 8122−8123.
(4) Well-ordered superlattices have been prepared by the evaporation of organic solvents from nanoparticles stabilized by nonpolar ligands, although this method is incapable of placing an arbitrary variety of distinct particles in predetermined locations. For a review, see Murray, C. B.; Kagan, C. R.; Bawendi, M. G. *Annu. Rev. Mater. Sci.* **2000**, *30*, 545−610.
(5) Elghanian, R.; Storhoff, J. J.; Mucic, R. C.; Letsinger, R. L.; Mirkin, C. A. *Science* **1997**, *277*, 1078−1081.
(6) Jin, R.; Wu, G.; Li, Z.; Mirkin, C. A.; Schatz, G. C. *J. Am. Chem. Soc.* **2003**, *125*, 1643−1654.
(7) (a) Nielsen, P. E.; Egholm, M.; Buchardt, O. *Bioconjugate Chem.* **1994**, *5*, 3−7. (b) Eriksson, M.; Nielsen, P. E. *Q. Rev. Biophys.* **1996**, *29*, 369−394. (c) Uhlmann, E.; Peyman, A.; Breipohl, G.; Will, D. W. *Angew. Chem., Int. Ed.* **1998**, *37*, 2796−2823. (d) Nielsen, P. E.; Egholm, M. *Curr. Issues Mol. Biol.* **1999**, *1*, 89−104.

10.1021/ja035399g CCC: $25.00

DNA duplexes, especially for short sequences, and (2) greater mismatch sensitivity. Furthermore, unlike the sugar−phosphate backbone, the polyamide one can be easily altered, for example, by using other amino acids in place of glycine,[8] allowing one to tune the structural and electrostatic properties of the molecule to exert control over the dynamics of assembly. Besides their applications to nanofabrication, PNA−nanocrystal conjugates might offer advantages over DNA-modified nanoparticles in the domain of nanoscale sensing, wherein the enhanced base pair mismatch selectivity of PNA may improve the discrimination of the sensors for a target sequence in the presence of a nonspecific background.

Motivated by these prospects, we investigated the properties of PNA-modified gold nanocrystals and studied their programmed assembly into macroscopic aggregates. As we will show, there are significant difficulties encountered in conjugating standard PNA structures to nanoparticles, necessitating the use of unconventional PNA motifs. Factors affecting the surface densities and hybridization efficiencies of these motifs were systematically examined, and effects of nanosurface curvature were identified. We explored applications of these conjugates to sensing and found an unexpected mode of selective DNA detection only possible with PNA-modified particles. Finally, we assembled the conjugates by means of various combinations of PNA and DNA interactions and analyzed the effects of PNA length, mismatch selectivity, and charge distribution on the specificity and dynamics of growth.

Results and Discussion

Design of PNA Structures Compatible with Nanocrystal Stability. Because of PNA's neutrality, the introduction of charge through basic or acidic residues at the polymer termini can dramatically affect its electrostatic properties. The net surface charge density of the nanoparticles, and hence their stability, is determined by the sum of the charges on the PNA ligands and those on the small molecules coating the gold surface. We examined different PNA charge distributions (see Table 1 for a list of structures employed) to determine their effects on nanoparticle stability.

Conjugates prepared using simple citrate-stabilized nanoparticles and standard PNAs A or B underwent immediate irreversible agglomeration due to the uncapped N-terminal amines whose positive charge at neutral pH decreases the negative surface charge density. PNAs A or B presented additional complications due to the tendency of the excess PNA to self-aggregate and pellet during the centrifugation process. In PNA C, we neutralized the N-terminal amine by acetylation and placed four extra "O" linker moieties between the cysteine and the PNA sequence. The resultant extra hydrophilicity rendered this polymer resistant to centrifugation-induced aggregation.

To determine the feasibility of conferring greater electrostatic stabilization upon PNA-coated nanoparticles, we examined the properties of negatively charged peptide−PNA chimeras. In PNA D, a single anionic glutamic acid residue was appended to the distal end of a structural motif similar to PNA C. By contrast, when polyanionic groups were used, they were incorporated at the tethered end to minimize interference with hybridization. PNA E was 12 bases in length with three glutamic acid residues at the proximal terminus. To examine whether very short PNAs could hybridize effectively on the surfaces of nanoparticles, we studied the properties of PNA F, six bases in length[9] with three aspartic acid residues at its tethered end.[11]

Table 1. PNA and DNA Sequences Used

designation	sequence[a]
PNA A	Cys-O-ATG CTA CGG ACT TGT AAC-am
PNA B	Cys-O-CAG TGT CAG TTA CAA GTC-am
PNA C	Ac-TAG CAC TGA CCT TTC TTT-O_5-Cys-am
PNA C no thiol	Ac-TAG CAC TGA CCT TTC TTT-O_5-am
PNA D	Ac-Glu-GTC AGT GCT ACT TTC TTT-O_5-Cys-am
PNA D2	Ac-Cys-O_5-TTT CTT CGG ACT TGT AAC-Glu-am
PNA E	Ac-Cys-Glu-Glu-Glu-O-CGG ACT TGT AAC-am
PNA E2	Ac-GTC AGT GCT ACT-O-Glu-Glu-Glu-Cys-am
PNA F	Ac-Cys-Asp-Asp-Asp-O-GCC GCC-am
PNA Cy-C	Cy3-O_2-TAG CAC TGA CCT TTC TTT-O_5-Cys-am
PNA Cy-D	Cy3-O-Glu-GTC AGT GCT ACT TTC TTT-O5-Cys-am
PNA Fam-E	Ac-Cys-Glu-Glu-Glu-O-CGG ACT TGT AAC-O-Lys/Fam[b]
PNA Fam-F	Ac-Cys-Asp-Asp-Asp-O-GCC GCC-O-Lys/Fam[b]
PNA DE	Ac-CAC TGA CTG TTA CAA-am
DNA D	5′ GTC AGT GCT ACT AAA-C_3 thiol 3′
DNA E[c]	5′ C_6 thiol-AAA CGG ACT TGT AAC 3′
DNA G[c]	5′ TGC GAG TTG TAG-C_3 thiol 3′
DNA Cc	5′ GTC AGT GCT A-Fam 3′
DNA Ec	5′ Fam-GTT ACA AGT CCG 3′
DNA Emis	5′ Fam-GTT ACA A**C**T CCG 3′
DNA Fc	5′ Fam-ATT TGG CGG C 3′
DNA CE	5′ GTC AGT GCT AGT TAC AAG TC 3′
DNA DE[d]	5′ TAG CAC TGA CAA GTT ACA AGT C 3′
DNA DEmis	5′ TAG CAC TGA CAA GTT ACA A**C**T C 3′
BSPP	Ph-P-(C_6H_4−SO_3K)$_2$

[a] All PNAs are written from N to C terminus. Ac = acetyl; am = amide; Fam = 6-carboxyfluorescein; O_n refers to an *n*mer of the linker unit (−NH−CH_2−O−CH_2−CH_2−O−CH_2−CO−). [b] For C-terminal labeling with Fam, a Lys residue was incorporated during synthesis to facilitate conjugation with Fam NHS ester. [c] Versions of these DNAs labeled with Fam at their distal ends were also prepared for fluorescence assay. [d] Version with Fam at 3′ end used for fluorescence assay.

Despite the greater hydrophilicity and more favorable charge properties of these modified PNAs, their citrate gold conjugates were not stable for extended time periods (Table 2). Conjugate stability was enhanced by treating citrate-stabilized gold particles with *p*-bis-sulfonatophenyl(phenylphosphine) (BSPP).[13] The resultant nanoparticles withstood treatment with arbitrarily high concentrations of PNAs D and E at 10 mM Na^+ without agglomeration or any red-shift in the Au surface plasmon band at 520 nm. Treatment with PNA C at 10 mM Na^+ resulted in some plasmon red-shift, consistent with its neutrality; treatment with PNAs A or B caused a greater red-shift, and the conjugates began to precipitate within 2−3 days (Table 2). Because of their destabilizing effects, even in the presence of BSPP, PNAs A and B were excluded from subsequent studies.

With the notable exception of PNA F, conjugates of PNAs with BSPP−Au nanoparticles all irreversibly agglomerated to some degree above 20 mM Na^+ over time; BSPP−Au or even plain citrate−Au conjugates of PNA F were stable up to 50

(8) Ganesh, K. N.; Nielsen, P. E. *Curr. Org. Chem.* **2000**, *4*, 941−943.

(9) Although 6mer DNA−DNA duplexes are, at best, marginally stable at room temperature, even a poly-dT/poly-dA 6mer PNA−DNA duplex has a T_m > 30 °C.[10]

(10) Egholm, M.; Buchardt, O.; Nielsen, P. E.; Berg, R. H. *J. Am. Chem. Soc.* **1992**, *114*, 1895−1897.

(11) In solution, the pK_a of aspartic acid is 3.9, compared to 4.3 for glutamic acid; the more acidic aspartic acid is expected to be more thoroughly deprotonated on surfaces, where pK_a's can increase by up to 2 units.[12]

(12) Fritz, J.; Baller, M. K.; Lang, H. P.; Strunz, T.; Meyer, E.; Guntherodt, H.-J.; Delamarche, E.; Gerber, C.; Gimzewski, J. K. *Langmuir* **2000**, *16*, 9694−9696.

(13) Loweth, C. J.; Caldwell, W. B.; Peng, X.; Alivisatos, A. P.; Schultz, P. G. *Angew. Chem., Int. Ed.* **1999**, *38*, 1808−1812.

Table 2. Stability of PNA−Nanocrystal Conjugates: Effect of Surface Charge Distribution

PNA sequence[a]	citrate–Au conjugate stability[b] (10 mM Na^+)	BSPP–Au conjugate stability[c] (10 mM Na^+)	maximum [Na^+] BSPP–Au conjugate (mM)[d]
A	immediate precipitation	red-shift, $\lambda = 529$ nm[e]	10
C	precipitates (2 min)	red-shift, $\lambda = 524$ nm[e]	20
D	precipitates (10 min)	indefinitely stable	20
E	precipitates (10 min)	indefinitely stable	20
F	indefinitely stable	indefinitely stable	50

[a] Only distinct structural motifs are listed; stability of PNA: A = B, D = D2, E = E2. [b] Citrate−Au nanoparticles were indefinitely stable up to 40 mM Na^+. [c] BSPP−Au nanoparticles were indefinitely stable up to 120 mM Na^+. [d] Precipitation occurs at higher [Na^+]. [e] Shift of Au surface plasmon band from $\lambda = 520$ nm, indicating particle agglomeration, upon addition of 0.6 μM PNA to 10 nM nanoparticles.

Table 3. Gold Thin Film Surface Coverage by Various PNA Monolayers[a]

PNA sequence	supplementary treatment[b]	[Na^+] (mM)	PNA surface density[c] (pmol/cm^2)
E	BSPP	500	26
F	BSPP	500	44
C	BSPP	10	42
D	BSPP	10	41
DNA E	none	500	15

[a] [PNA] in deposition solution = 2 μM. [b] Supplementary treatment of nanoparticles with BSPP was carried out prior to PNA adsorption. [c] The data presented in each case are the mean values calculated from five independent assays; the standard deviation in no instance exceeded 10%.

mM Na^+. However, as discussed below, when nanoparticles modified with any of the above PNAs were hybridized to DNA, or when mixed PNA/DNA monolayers were used, resistance to elevated salt concentrations improved considerably.

These results indicate that hydrophobic interactions, as well as charge density, affect the stability of PNA-modified nanocrystals. External charge, as in PNA D, deters hydrophobic attraction and confers extra stability. Having ascertained the effects of PNA structural features on conjugate stability, we undertook a thorough investigation of surface coverage and hybridization properties of these polymers. To better understand these properties and to determine the effects of nanosurface curvature, we examined the characteristics of monolayers composed of the representative PNA motifs on both gold thin films and nanoparticles.

Surface Coverage by PNA Monolayers: Effects of Nanosurface Curvature. The surface coverages of PNAs on thin films were determined using either fluorescence or XPS (see Experimental Section). The maximal surface coverages are listed in Table 3. Figure 1 displays the variation of XPS peak area with salt concentration; for simplicity, N 1s peak areas are normalized to the maximal peak area of DNA E. The maximal surface coverages for PNAs C, D, and E and DNA E follow the trend expected on the basis of total charge, while the shorter, more rigid PNA F experiences less steric repulsion and packs more tightly than its charge suggests. The surface densities of PNA C and D exhibited virtually no dependence on salt concentration (Figure 1), indicating that a distal negative charge does not decrease surface coverage. By contrast, the N 1s peak area for PNA E, bearing negative charges at its tethered end, more than doubles between 10 and 300 mM Na^+; the effect was even more dramatic for PNA F because of the greater acidity of aspartic acid versus glutamic acid residues.

Table 4 lists the surface coverages on nanoparticles under various conditions, all measured using the fluorescein/Cy3-based method; a more limited range of salt concentrations was studied

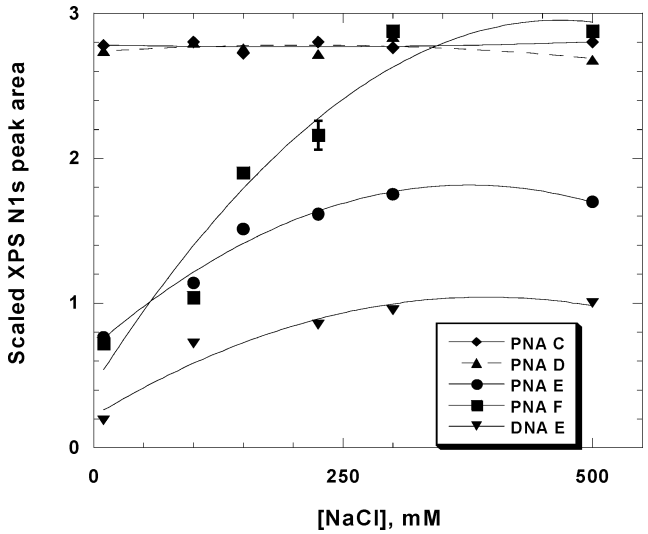

Figure 1. Salt dependence of thiolated PNA surface coverage on gold thin films. XPS peak areas for each PNA are scaled by surface coverage measured by fluorescence assay at 500 mM (E, F, DNA A) or 10 mM (C, D) NaCl; maximal DNA E surface coverage normalized to 1. The error bar shown is representative of the random errors involved in analysis.

compared to gold films because of the sensitivity of PNA−nanoparticle stability to salt. Comparison of the thin film and nanoparticle surface coverage data provides insight into the effects of nanosurface curvature on PNA monolayers. The surface density of PNA E at 10 mM Na^+ is much greater on nanoparticles (60 pmol/cm^2; Table 4) than on thin films (~12 pmol/cm^2 estimated from XPS; Supporting Information, Table 1S). The relative increase in coverage is similar to that observed with DNA. Since the charges on DNA are distributed over the whole thickness of the monolayer, while those on PNA E are very close (<~1 nm) to the surface, the increased densities on nanocrystals must originate primarily from charge separation near the surface. This is noteworthy, since nanoparticle curvature increases the separation of distal charges more so than those nearby. For PNA D, the relative increase in surface density on nanoparticles compared to thin films (Tables 3 and 4) is below that of PNA E; PNA D is uncharged near the surface and, hence, moving to the nanosurface does not offer the same relief in electrostatic repulsion.

We examined the effect of increasing salt concentration (50, 75, and 100 mM) on the nanosurface density of PNA E by using a lower PNA concentration to avoid surface saturation. Although increased salt concentrations result in greater surface coverage, conjugates prepared at elevated [Na^+] (above 50 mM for fluorescein-labeled E and above 20 mM for unlabeled E) were unstable over extended periods of time. The inability to obtain greater surface densities by raising the salt concentration is of

Table 4. Gold Nanoparticle Surface Coverage by PNA Monolayers Prepared under Various Conditions

PNA sequence	prep	supplementary treatment[a]	[PNA] (μM)	[Na^+] (mM)	PNA surface density[b] (pmol/cm^2)	PNA strands/particle
E	I	BSPP	5	10	60	190
	IIa	BSPP	2.5	50	35	110
	IIb	BSPP	2.5	75	54	170
	IIc	BSPP	2.5	100	70	222
F	III	none	5	10	54	170
D	IV	BSPP	3	10	64	200
DNA E	V	none	3	100	47	150
DNA E/post PNA C[c]	VI	none	3 (DNA)/3 (PNA)	100/10	26 (DNA)/35 (PNA)	81 (DNA)/110 (PNA)

[a] Supplementary treatment of nanoparticles with BSPP was carried out prior to PNA adsorption. [b] See footnote 3 to Table 3. [c] PNA deposited after DNA deposition and purification.

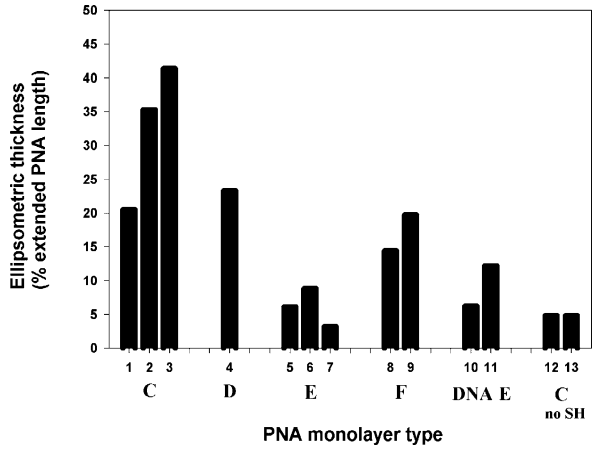

Figure 2. Ellipsometric thicknesses of PNA monolayers formed on gold thin films under various conditions. Extended PNA length is defined as twice the length of the corresponding double helix.[14] All monolayers were deposited at 2 μM PNA and 5 mM PB (10 mM Na^+) unless otherwise stated. PNA C: (1) on BSPP-treated gold; (2) 9 μM PNA on BSPP-treated gold; (3) 9 uM PNA on bare gold. PNA D: **(**4) on BSPP-treated gold. PNA E: **(**5) 10 mM Na^+ on BSPP-treated gold; (6) 100 mM Na^+ on BSPP-treated gold; (7) 10 mM Na^+ on BSPP- and mercaptosuccinic acid (MSA)-treated gold. PNA F: **(**8) 100 mM Na^+ on BSPP-treated gold; (9) 500 mM Na^+ on BSPP-treated gold. DNA E: **(**10) 100 mM Na^+ on bare gold; (11**)** 500 mM Na^+ on bare gold. Unthiolated PNA C: (12) 10 mM Na^+ on BSPP-treated gold; (13) on BSPP- and MSA-treated gold. MSA enhances the hybridization efficiency of PNA monolayers (see Supporting Information).

little practical consequence, since coverages at 10 mM are already higher than those obtained with DNA at 100 mM. Similar nanosurface coverages were obtained with PNA F at 10 mM Na^+ (Table 4).

To structurally characterize PNA monolayers bearing various charge distributions, we measured their ellipsometric thickness on thin films under different deposition conditions (Figure 2). Thicknesses were expressed as a percentage of the length that would be expected if the polymers were standing extended and normal to the surface.[14] Notably, raising the concentration of PNA C (or D, data not shown) from 2 to 9 μM increased the monolayer thickness considerably (Figure 2, lanes 1 and 2), although the XPS N 1s peak area only increased by 12% (Supporting Information, Table 1S), suggesting that PNAs with neutral tethered ends may undergo a phase transition to a state where the polymers are more ordered and erect. This behavior was not observed with PNAs bearing charged tethered ends; indeed, the similar relative thickness of DNA E, PNA E, and PNA F monolayers deposited at high salt indicates that the configurational properties of DNAs and these PNAs in maximally dense monolayers are not fundamentally different, although the PNA surface densities are considerably greater.

Nanoparticle Stabilization via PNA/DNA Mixed Monolayers. Because of the relatively low salt stability of pure PNA-coated nanoparticles, even in the presence of BSPP, we examined methods for the preparation of mixed monolayers composed of both PNA and DNA. Polyelectrolytes are most effective for conferring additional stability to aqueous nanoparticle suspensions, since they introduce the greatest charge density per surface area and do not experience any hydrophobic attraction. We chose to use DNAs because oligos of controlled lengths can be cheaply and readily synthesized and because their structural similarity to PNAs allowed further insight into the role of nucleic acid charge distribution on nanoparticle stability.

We first studied the effects of adding the PNA to a preformed monolayer of DNA.[15] This method was satisfactory for proximally neutral PNAs (e.g., C; Table 4), but proximally charged PNAs (e.g., E) were less effective at displacing DNA monolayers. For the latter, coadsorption[16] of PNA and DNA from the same solution gave better results. Monolayer compositions resulting from coadsorption of various PNA:DNA ratios at 10 mM Na^+ are displayed in Figure 3. We found that the optimal preparative strategy is coadsorption of the PNA with an excess of DNA (6:2 μM DNA E:PNA E) at 10 mM Na^+ to ensure that the conjugate has sufficient salt stability, followed by elevation of the salt concentration (to ~100 mM) to decrease electrostatic repulsion and allow enough PNA to adsorb to the surface. Conjugates prepared in this way were indefinitely stable above 100 mM Na^+, and the method was employed in the assembly of PNA-coated nanoparticles by means of a DNA linker (below).

Hybridization Properties of PNA-Modified Nanoparticles and Thin Films. We first studied the dependence of PNA−DNA hybridization efficiency on electrolyte concentration, using thin films rather than nanoparticles, to determine to what extent hybridization efficiencies are limited by particle stability; on nanoparticles, PNA hybridization assays were not carried out above 150 mM Na^+ (see below). These data are provided as Supporting Information (Figure 2S). In short, the hybridization of DNA to PNA C monolayers was least sensitive to salt because of the neutrality of this PNA (plateau around 80 mM Na^+); the presence of single (PNA D) or multiple (PNA E) negative charges increases the salt concentration for maximal hybridization (to 150−175 mM and 250 mM Na^+, respectively), and the

(14) Herne, T. M.; Tarlov, M. J. *J. Am. Chem. Soc*. **1997**, *119*, 8916−8920.

(15) The treatment of preformed PNA D monolayers on thin films with DNA E at 100 mM Na^+ resulted in essentially no attachment of DNA (data not shown). This method was therefore not applied to nanoparticles.

(16) Bain, C. D.; Evall, J.; Whitesides, G. M. *J. Am. Chem. Soc*. **1989**, *111*, 7155−7164.

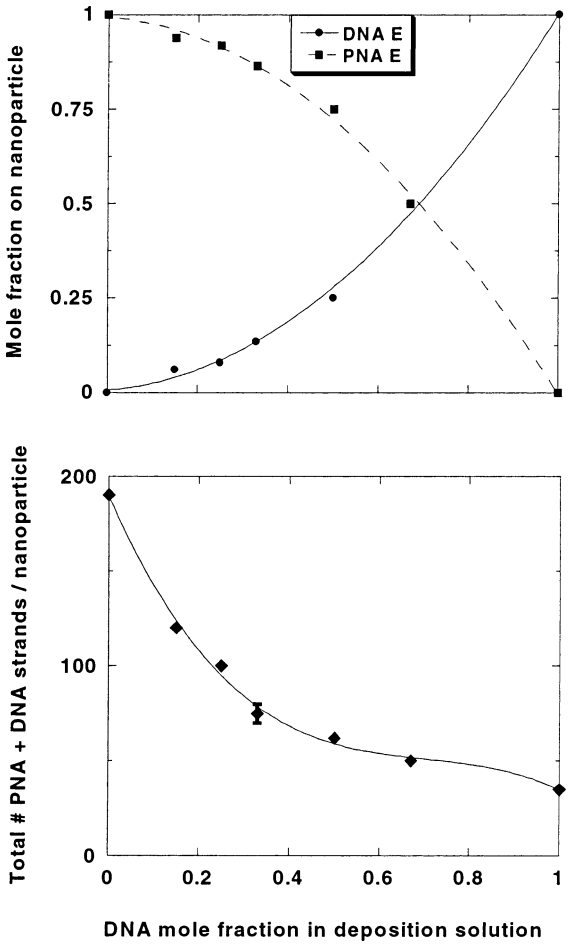

Figure 3. Coadsorption of various ratios of DNA E and PNA E onto gold nanoparticles in 5 mM PB (10 mM Na^+, pH 7.3). The error bar shown is representative of the random errors involved in analysis.

lower stability of short duplexes (PNA F) imposes limits on the hybridization efficiency that cannot be overcome by increasing the salt (plateau 150−175 mM Na^+ despite triple charge).[17]

Efficiencies of hybridization of PNA monolayers on thin films to various fluorescein-labeled DNAs are listed in Table 5. Table 6 lists the surface density of fluorescein-labeled DNAs hybridized to PNA-coated nanoparticles prepared under various conditions listed in Table 4. The hybridization efficiencies of the various PNAs on thin films are typically considerably lower than those on nanoparticles at identical salt concentrations. The greater hybridization efficiencies observed on nanoparticles, despite the higher surface densities of immobilized PNAs (Tables 2 and 3), appear to result from a relief of steric occlusion[18] due to the surface curvature.

Because of the detrimental effect of high salt concentrations on particle stability, we investigated the use of small molecules to enhance hybridization efficiencies at low ionic strength. Mercaptosuccinic acid was especially effective in this regard (see Supporting Information for details).

To determine whether the high stability of PNA duplexes would allow the effective hybridization of very short immobilized sequences, we examined the hybridization efficiency of the 6mer PNA F (Table 6). For many materials applications, the interesting physical properties depend critically on collective particle interactions, which are strongest at small separation distances.[4] Although the hybridization efficiency (3%, five hybridized strands per particle) was below those of the longer sequences studied, it is roughly equal to the previously reported value of six hybridized strands per particle for a 12mer DNA that was sufficient to direct nanoparticle assembly.[19] By comparison, only 1% hybridization was achieved with PNA F monolayers on thin films (Table 5).

Single Base Mismatch Discrimination. The mismatch selectivity of PNA hybridization on nanoparticles and thin films was studied by comparing the hybridization efficiencies of a perfectly complementary 12mer and an identical 12mer bearing a single base mismatch to PNA E (Tables 5 and 6). Interestingly, the selectivity ratio on nanosurfaces (∼14:1) exceeds that on thin films (∼7:1). It has been postulated that the low permeability of PNA monolayers on thin films enhances mismatch selectivity by inhibiting the binding of mismatched DNA more so than complementary DNA.[20] The selectivity of this mechanism can be improved on nanosurfaces if the surface curvature spaces out the recognition sites to a distance that improves the binding of complementary sequences, while still inhibiting the binding of mismatched sequences.

The melting temperatures (T_m's) of PNA−DNA hybrids bearing a single base mismatch are typically 10−15 °C lower than those of the corresponding DNA−DNA hybrids.[7] The mismatch selectivity of PNA E-coated nanoparticles was some 5 times greater than that of DNA E-modified nanoparticles (Table 6). These results demonstrate that the signficantly greater mismatch selectivity of PNA is not only retained but enhanced on nanosurfaces, making PNA−nanoparticle conjugates the preferred medium for defect-free self-assembly or highly selective nanosensing (see below).

DNA Hybridization-Induced Stabilization: Colorimetric Mismatch Detection. The hybridization of DNA to PNA-coated nanoparticles increases the salt stability of these conjugates, often dramatically. Although none of the pure PNA−nanoparticle conjugates examined are stable above 40 mM Na^+, upon heavy hybridization to complementary DNA many resisted salt-induced agglomeration even beyond 200 mM Na^+. Clearly, the additional surface charge imparted by bound DNA increases the electrostatic stabilization of the colloids. The extent of this DNA-induced stabilization was found to be sensitive to the hybridized surface density. In particular, PNA E−DNA Emis hybrids rapidly agglomerated above 160 mM Na^+, while PNA E−DNA Ec hybrids were stable for days up to 200 mM Na^+. This sensitivity of particle stability to target DNA sequence thus constitutes a novel, nanoparticle-based colorimetric DNA detection method, wherein PNA−nanoparticle conjugates are incubated with the DNA sequence of interest, and the salt concentration is then raised to a level where matched hybrids are stable but mismatched hybrids undergo agglomeration. Because of the exceptional base pair mismatch selectivity of PNA and the rapid time course of agglomeration, this method permits the colorimetric discrimination of single base mismatches on very short

(17) In these studies, all monolayers were deposited under conditions that resulted in dense surface coverage of the tethered polymer (2 μM PNA, 500 mM Na^+ for E, F, and DNA G).
(18) Aoki, H.; Buhlmann, P.; Umezawa, Y. *Electroanalysis* **2000**, *12*, 1272−1276.
(19) Demers, L. M.; Mirkin, C. A.; Mucic, R. C.; Reynolds, R. A.; Letsinger, R. L.; Elghanian, R.; Viswanadham, G. *Anal. Chem.* **2000**, *72*, 5535−5541.
(20) Wang, J. *Biosens. Bioelectron.* **1998**, *13*, 757−762.

Table 5. Hybridization Efficiencies of PNA Monolayers on Gold Thin Films

PNA sequence in monolayer	PNA surface density in monolayer[a] (pmol/cm)[b]	hybridized DNA sequence	[Na^+] during hybridization (mM)	hybridized surface density[b] (pmol/cm^2)	% PNA strands hybridized
E	26	Ec	150	1.9	7
	26	Emis[c]	150	0.2	1
F	44	Fc	150	0.6	1
C	42	Cc	100−200[d]	4.3	10
D	41	DE	150	1.3	3
DNA E	15	Ec		2.9	19

[a] All hybridization assays were carried out using PNA monolayers deposited at the highest possible surface densities (see Table 4). [b] The data presented in each case are the mean values calculated from five independent assays. [c] Emis is a single base mismatch mutant of Ec. [d] Tested in 25 mM increments.

Table 6. Hybridization Efficiencies of PNA Monolayers on Gold Nanoparticles

PNA sequence in monolayer	conjugation conditions[a] [# PNA/particle]	hybridized DNA or PNA sequence	[Na^+] during hybridization (mM)	hybridized surface density[b] (pmol/cm^2)	PNA strands hybridized per particle	% PNA strands hybridized
	I [190]	Ec	150	8.1	26	14
E	I [190]	Emis[c]	150	0.6	2	1
	I [190]	PNA DE	10	51	160	84
F	III [170]	Fc	150	1.7	5	3
D	IV [200]	DNA DE	150	12	38	19
DNA E/post PNA C	VI [110]	Cc	100	11	35	32
DNA E	V [150]	Ec	300	12	37	25
	V [150]	Emis	300	4.1	13	9

[a] See Tables 3 and 4 for definitions of conjugation conditions. [b] Hybridization efficiencies were determined by fluorescence assay using FAM-labeled target strands, except for PNA DE where the immobilized PNA E was FAM-labeled (see Experimental Section). The data presented in each case are the mean values calculated from five independent assays; the standard deviation did not exceed 10% (except for the second entry). [c] Emis is a single base mismatch mutant of Ec.

Table 7. Comparison of Assembly Rates and Spectral Properties of Gold Nanoparticle Aggregates Formed by Representative Combinations of PNA and DNA Interactions

nanoparticle system[a]	linker	assembly conditions	time for precipitation	final[b] λ_{max} (nm)
[PNA C/DNA G]−[PNA D2/DNA G]	DNA AC	RT	∼15 hr	535
[PNA E/DNA G]−[PNA E2/DNA G]	DNA DE	RT	∼12 hr	537
[PNA E/DNA G]−[PNA E2/DNA G]	DNA DEmis[c]	RT	no precipitation[d]	520 (no change)
PNA E2−PNA D2	PNA DE	−78 °C (1 h), then RT[e]	∼5 days	533
DNA E−DNA D	PNA DE	−78 °C (1 h), then RT[e]	no precipitation[d]	520 (no change)
DNA E−DNA D	DNA AD	RT	∼2 hr	542

[a] Brackets indicate mixed monolayers; underline designates species in mixed monolayer that hybridize to linker. Mixed monolayers were prepared by post-treatment of DNA G-coated particles with the respective PNAs. [b] λ_{max} refers to the peak position of the gold nanoparticle surface plasmon band; the initial value prior to assembly was ∼520 nm in each case. [c] DEmis is a single base mismatch mutant of DE. [d] No precipitation was observed over 2 weeks. [e] These systems were frozen in a dry ice/isopropyl alcohol bath for 1 h to initiate assembly, thawed, and allowed to continue assembly at RT.

time scales (<10 min). Note that DNA detection on the basis of particle stability is not possible with DNA−nanoparticle conjugates because their salt stability does not change appreciably upon the hybridization of additional DNA.

PNA−PNA Hybridization on Nanosurfaces. Although the majority of hybridization studies were carried out using DNA targets, we also studied the hybridization of PNA E-coated nanoparticles to a complementary 15mer PNA strand bearing a 7-base recognition site (at 10 mM Na^+) (Table 6). Significantly, the level of PNA hybridization was found to far exceed (84% immobilized strands) that of any of the DNAs studied, showing that even very dense packing of PNA on nanosurfaces does little to inhibit binding in the absence of any electrostatic repulsion. Since PNA−PNA hybridization offers high hybridization efficiencies at low salt concentrations, even for short recognition sequences, it allows the assembly PNA-coated nanoparticles under conditions where they are most stable and presents an attractive route to the generation of materials with short interconnects (see below).

PNA-Directed Nanoparticle Assembly. PNA interactions can, in principle, direct nanoparticle assembly in several ways. Particles coated with monolayers of pure PNA, mixed PNA/DNA, or pure DNA can be assembled by either PNA or DNA linker strands. We explored each of these modes of assembly using various combinations of the sequences assayed above. Assembly rates and spectral properties of the aggregates formed in some representative experiments are summarized in Table 7. These examples have been chosen to highlight the advantages conferred by the superior duplex stability and mismatch selectivity of PNA and to demonstrate the effect of PNA charge distribution on the dynamics of assembly.

The assembly of pure PNA-coated particles using DNA linkers was subject to the important constraint that the comparatively low surface charge density of these particles, in the absence of heavy DNA hybridization, renders them unstable above 20 mM Na^+. The efficiency of DNA hybridization below 20 mM is low. Although the electrostatic barrier to the particle−particle approach is also low, attempts to assemble either pure PNA E2-coated particles with pure PNA D2-coated ones or pure PNA E-coated particles with pure PNA E2-coated ones with the DNA linker DE were not successful. On the other hand, because the hybridization of free PNA to PNA monolayers can

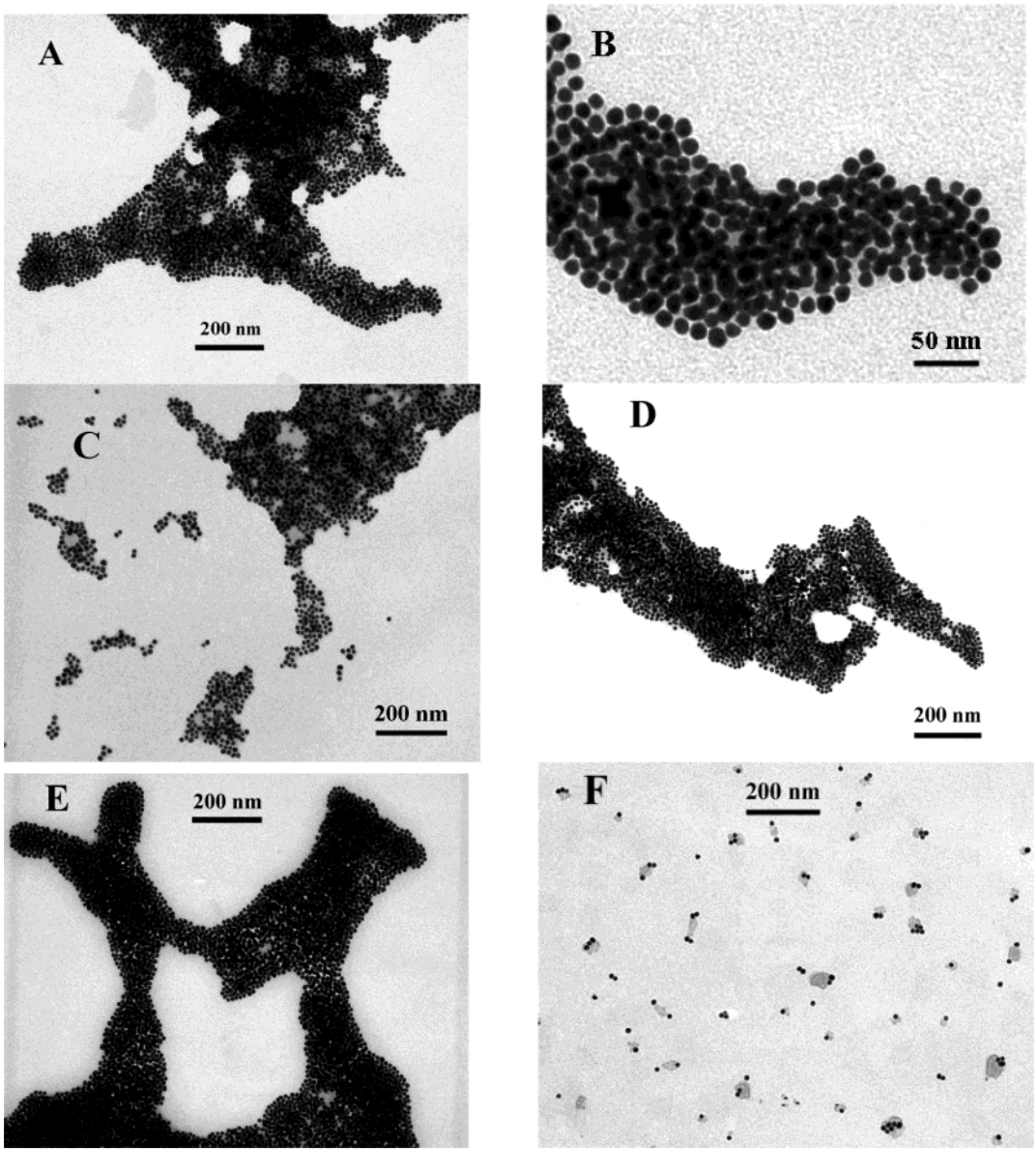

Figure 4. TEM micrographs of gold nanocrystals assembled by representative combinations of PNA and DNA interactions. (A) PNA E2-coated nanoparticles assembled with PNA D2-coated ones by the 15 base linker PNA DE (assembly facilitated by cooling to −78 °C followed by thawing to room temperature). (B) Higher magnification image of a section from A. (C) Mixed PNA C/DNA G-coated nanoparticles assembled with mixed PNA D2/DNA G-coated ones by the 20 base linker DNA CE (complementary to PNAs C and D2); the DNA linker was prehybridized to the PNA C/DNA G particles prior to assembly. (D) Mixed PNA E 2/DNA G-coated nanoparticles assembled with DNA E-coated ones using the 20 base pair linker DNA DE (complementary to DNA E and PNA E2). (E) DNA E-coated nanoparticles assembled with DNA D-coated ones by the linker DNA DE. (F) Unmodified gold nanocrystals. In C and D, mixed monolayer-coated nanoparticles were prepared by post-treatment of DNA G-coated ones with the respective PNAs.

occur with very high efficiency at low salt (Table 6), pure PNA-coated nanoparticles can be assembled by PNA linkers.

Assembly by PNA−PNA Hybridization. Upon the addition of a ∼40-fold molar excess of the linker PNA DE (15 bases, seven base recognition sites) to an equimolar mixture of pure PNA E2-coated and pure PNA D2-coated particles, no change in the surface plasmon band was detected over 12 h. However, after freezing the mixture to −78 °C for 1 h and thawing, the color of the solution changed from burgundy red to reddish-purple, with a shift in the surface plasmon band from ∼520 to ∼529 nm. Over the course of 5 days, essentially all of the nanoparticles precipitated. The plasmon band of the final aggregates (redispersed by agitation) shifted to 535 nm. Control experiments in which the particles were combined, frozen, and thawed without linker or in which an identical concentration of linker was added to the individual particle suspensions followed by freezing and thawing resulted in no detectable changes. TEM images of the aggregates (Figure 4, parts a and b) revealed few isolated nanoparticles; high magnification (b) suggested the particles did not fuse, despite being closely spaced. By contrast, particles coated with pure monolayers of DNA E and DNA D combined as above in the presence of the linker PNA DE showed no spectral shift or precipitation even after freezing and thawing. Attempts to assemble DNA−nanoparticle conjugates via a DNA linker with seven base recognition sites were also unsuccessful.

The requirement of low temperatures to facilitate assembly of the pure PNA system, despite the efficient hybridization of PNA E2-coated particles to this linker at RT (Table 6), indicates that the electrostatic barrier to particle approach is high enough

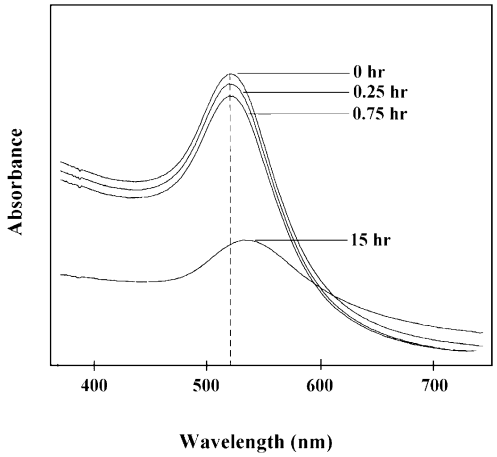

Figure 5. Time-dependent changes in the gold nanoparticle surface plasmon band during the assembly of mixed PNA C/DNA G-coated nanoparticles with PNA D2/DNA G-coated ones by the 20 base linker DNA CE (complementary to PNAs C and D2). Note that in the early stages of assembly there is a decrease in band intensity but no detectable wavelength shift. By 15 h, the majority of particles had precipitated and the band was noticeably red-shifted (the spectrum at 15 h was taken after agitation to redisperse aggregates). TEM images of the aggregates formed in this system are shown in Figure 4c.

even at these low surface charge densities to inhibit the formation of aggregates at 10 mM Na^+. Freezing may initiate assembly by forcing the particles into close proximity, overcoming the initial barrier to the formation of aggregate nuclei.[3]

Assembly by PNA−DNA Hybridization. Since DNA linker-directed assembly requires particle stability at moderate salt concentrations, the use of mixed PNA/DNA monolayers was necessary. In one system studied, assembly of particles coated with DNA G/PNA C and DNA G/PNA D2, respectively, was achieved. These particles were prepared by the treatment of DNA G-coated particles with 1.5 μM PNAs C or D at 10 mM Na^+. The PNA C particles were first prehybridized with a saturating concentration of DNA linker CE (to confer sufficient salt stability), followed by purification and combination with the PNA D2 particles at 100 mM Na^+. During the initial hour of assembly, the intensity of the plasmon band decreased, accompanied by visible paling of the solution but no wavelength shift. However, after 15 h most of the particles had precipitated and upon redispersion exhibited a red-shift in their plasmon band to 535 nm (Figure 5). TEM images of the pinkish precipitate (Figure 4c) revealed that although the majority of particles were present in aggregates, some were isolated or in small clusters.

In the assembly of distinctly different-sized nanoparticles by DNA−DNA interactions, similar changes were observed, including initial paling and slow assembly (24 h).[21] In that study, aggregates were incapable of growing beyond a small size because of particle-packing constraints. Herein, the small size of the aggregates may stem from low solubility in aqueous solution because of their low surface charge density. The slow rate of precipitation, common to all systems that result in small aggregates, can be attributed to the limited Ostwald ripening that occurs compared to systems with large aggregates where accelerated assembly takes place as the aggregates grow.[4]

Similar results were obtained with particles coated with DNA G/PNA E and DNA G/PNA E2, where the conjugates were prepared first by treating particles with a 6 μM DNA + 2 μM PNA for 12 h and then by raising [Na^+] to 100 mM. In this case, both particle types were sufficiently stable to salt that prehybridization was unnecessary; a 15−20-fold molar excess of the DNA linker DE was added to an equimolar mixture of the conjugates. Importantly, no assembly was detected when the single base mismatch mutant DNA DEmis was used as the linker. Attempts to assemble particles coated with distinctly different monolayers (for example, DNA G/PNA E with DNA G/PNA D) were unsuccessful. Therefore, it appears that for DNA-directed assembly of PNA-coated nanoparticles at room temperature, the particles must have similar surface properties. It was possible, however, to assemble particles coated with mixed monolayers of DNA G/PNA E2 with pure DNA E-coated nanoparticles (Figure 4d; details in Supporting Information).

For comparison, pure DNA E and pure DNA D-coated particles were assembled by the DNA linker DE at 100 mM Na^+. Assembly occurred faster in this case, with complete precipitation within 2 h, and the surface plasmon maximum shifted to 545 nm. TEM micrographs (Figure 4e) indicated aggregates with no isolated particles. The greater solubility of pure DNA-coated aggregates implies that they mature longer than PNA-containing aggregates, growing more quickly (and larger) by Ostwald ripening (note that the TEM images in Figure 4, focusing on small portions of the aggregates, are not intended to provide an accurate indication of the relative sizes).

The foregoing representative examples show that PNA interactions are capable of directing the assembly of nanoparticles in a variety of formats, with several unique advantages. The ability of PNA−PNA hybridization to assemble nanocrystals, at a recognition length (seven bases) where DNA−DNA mediated assembly was unsuccessful, is particularly noteworthy since it represents the first practical application of pure PNA−PNA interactions[22] and because it shows that shorter interparticle spacings are possible using PNA-directed assembly.

Another advantage of PNA-directed assembly is that particle aggregation does not occur in the presence of a single base mismatch. With DNA−nanoparticle conjugates, some shift in the surface plasmon band, and consequently some degree of assembly, often occurs even in the presence of base mismatches.[5] In sensing applications, this nonspecific shift renders it difficult to unequivocally read out the presence of a target DNA from the assembly process itself; a slow temperature ramping is necessary to melt mismatched aggregates, which decompose at lower temperatures than matched ones. Since no nonspecific assembly occurs with PNA-modified particles, such an approach is unnecessary. This difference can be attributed to two factors. First and most important, the enhanced base mismatch selectivity of PNA compared to DNA decreases the average number of hybridizable mismatched strands per particle to two (versus 13 for DNA), an insufficient number to generate three-dimensional networks of particles. Second, because aggregates of even perfectly matched PNA−nanoparticle conjugates are much smaller than those formed from DNA, whatever assemblies are formed by mismatched sequences are so small that they result in no detectable shift in the plasmon peak maximum. The superior mismatch selectivity of PNA should also minimize defective assembly in nanofabrication applications

(21) Mucic, R. C.; Storhoff, J. J.; Mirkin, C. A.; Letsinger, R. L. *J. Am. Chem. Soc.* **1998**, *120*, 12674−12675.

(22) Wittung, P.; Nielsen, P. E.; Buchardt, O.; Egholm, M.; Norden, B. *Nature* **1994**, *368*, 561−563.

involving the simultaneous assembly of multiple distinct nanoparticles, especially when particle interconnects are short. In these cases, different particles may be coded by sequences that differ in only one or two bases.

Finally, the rate of assembly and the size of the resulting aggregates are controlled by the PNA charge distribution. The assembly of PNA-coated particles is generally slower and results in smaller red-shifts, indicating the formation of smaller aggregates, than the assembly of pure DNA-coated particles, and the assembly of PNA conjugates with similar surface properties is more facile than that of dissimilar particles. These effects may depend on the solubility of mesoscopic aggregates and the hydrophobic clustering of like particles, and the ability to tune their magnitude is useful because aggregate structure and crystallinity depend on the dynamics of growth. Preliminary thermal dissociation experiments, which provide information regarding assembly dynamics, reveal that aggregate melting curves are highly sensitive to the PNA charge distribution. A thorough examination of these subtle phenomena, with an aim toward generating well-ordered assemblies, is in progress.

In summary, the unique properties of PNA-directed nanoparticle assembly support continued development of a "PNA nanotechnology" analogous to conventional DNA nanotechnology. The ease with which the polyamide backbone can be readily altered makes PNA the optimal structural family for the investigation of biomimetic, as opposed to biokleptic,[23] self-assembly, especially given the ever-growing library of PNA variants that are being designed by synthetic groups.[8]

Experimental Section

Gold Nanoparticle Preparation. Citrate-stabilized Au nanoparticles were prepared by standard reduction of $HAuCl_4$ with triNa citrate,[24] filtered through a 0.45-micron nylon filter (Osmonics), and assayed spectrophotometrically using the gold plasmon band absorption at 518−520 nm (extinction coefficient of $2.9 \times 10^8\ M^{-1}\ cm^{-1}$). Particle diameter (assessed by TEM, see below) was 13.0 ± 1.2 nm.

Preparation of Gold Thin Films. Single-crystal ⟨100⟩ silicon wafers were used as substrates for gold thin films. Details of film deposition and functionalization with bis-(*p*-sulfonatophenyl)phenylphosphine (BSPP) and mercaptosuccinic acid (MSA) are provided as Supporting Information.

PNA and DNA Synthesis. The PNA oligomers used in this work were either synthesized on an Expedite 8909 synthesizer with PNA upgrade software using standard PNA chemistry and reagents from Applied Biosystems or purchased from that vendor. (See Supporting Information for details.) DNA oligomers were synthesized by standard phosphoramidite chemistry on an ABI 391 PCRmate DNA synthesizer using reagents from Glen Research. Table 1 lists the PNA and DNA sequences used in this work.

A cysteine residue was added to either the N- or C-terminus of PNAs to provide the thiol necessary for immobilization to gold (alkylthiol linkers were used for DNAs). In select cases, an "O" linker group was inserted between PNA and non-PNA monomers to increase conjugation yield during synthesis or for other reasons detailed below.

Selected PNAs were labeled with fluorescein or the more hydrophilic sulfocyanine dye Cy3 for the purpose of quantitative fluorescence assays (see below). Cy3 was used with PNAs C and D because of the tendency of fluorescein to induce aggregation of longer PNAs. To minimize quenching, two non-PNA monomers (either "O" linkers or amino acid residues) were maintained between the dye and the PNA segment of the oligomer in each case. PNA DE and the unthiolated DNAs bore recognition sites complementary to segments of the thiolated PNAs or DNAs.

Preparation of PNA−Gold Nanocrystal Conjugates. PNA−Au nanocrystal conjugates were prepared by incubating 0.6−3 μM cysteine-modified PNAs (Table 1) with ∼10 nM Au nanoparticle suspensions (citrate-stabilized, BSPP- or MSA-modified) in 5 mM phosphate buffer for 12 h in nonstick siliconized microcentrifuge tubes. The PNA-modified nanoparticles were then centrifuged for 20 min at 12 500−14 000 rpm, depending on stability. The supernatant was removed, and then the pellet was washed 2−3 times with 5 mM phosphate buffer (∼20% loss). The final concentration of the modified nanoparticles was assessed by spectrophotometry.

Quantitation of Nanoparticle/Thin Film Surface Coverage by PNAs. The surface densities of PNAs on nanoparticles were determined using PNAs labeled with either 6-carboxyfluorescein (for PNAs of 12 or fewer bases) or Cy3 (for longer PNAs) at their distal ends. A solution of 0.2 M KCN and 2 mM $K_3Fe(CN)_6$ was added to a 10 nM suspension of fluorescein/Cy3-modified nanoparticles (in 5 mM phosphate buffer, pH 7.3) at a 1:5 (v:v) ratio. Within 30 min, the surface plasmon resonance absorption band of the particles at 520 nm disappeared, indicating that the gold particles had been completely digested. The pH of the solution was then readjusted to 7.3 with HCl and diluted with 5 mM phosphate buffer. The fluorescence (fluorescein: 494/518 nm excitation/detection; Cy3: 548/562 nm excitation/detection) of the resulting solutions, in conjunction with a calibration curve determined by adding known amounts of the PNA to dissolved bare nanoparticles, were used to quantify PNA. Normalized surface coverage values were then calculated by dividing by the particle surface area estimated from TEM imaging (see below). Relative proportions of PNA and DNA in mixed monolayers were determined by carrying out two successive fluorescence assays: one in which the PNA was labeled and the other in which the DNA was labeled.

For surface coverages of PNAs E and F on thin films, films modified with fluorescein-labeled PNAs were incubated in buffered solutions of either mercaptoethanol (24 mM, 48 h) or mercaptohexanol (10 mM, 15 h) to displace the PNAs for solution phase fluorescence detection. Films modified with Cy3-conjugated PNAs C or D were heated to 80 °C for 30 min in 20 mM mercaptohexanol and then slowly cooled to RT. Quantitative displacement was achieved within 48 h using this method. XPS was used to estimate PNA surface densities achieved under various deposition conditions because of its higher throughput. Although it is difficult to extract absolute surface coverages from XPS spectra,[25] the relative areas of the N 1s peak for a given PNA provide an approximate indicator of relative coverages.

Quantitation of Hybridization Efficiency of Nanoparticle/Thin Film-Immobilized PNAs. The surface density of hybridizable PNA strands tethered to gold nanoparticle or thin film surfaces was assayed by incubating purified PNA−gold conjugates with 3 μM complementary DNA modified at its distal end with fluorescein at a predetermined concentration of NaCl (in 5 mM phosphate buffer, pH 7.3) using a modification of a method previously described.[14] After 12 h at room temperature, the hybridized nanoparticles were purified by centrifugation at 13 000−14 000 rpm for 20 min, followed by washing 3 times with buffer at the identical salt concentration. The purified particles were then dehybridized from the labeled DNA by raising the pH to 11.5 for 2 h. The nanoparticles were separated from the DNA by centrifugation (14 000 rpm, 20 min), and the supernatant was adjusted to pH 7.3 with HCl and diluted with 5 mM phosphate buffer prior to quantifying hybridized DNA by fluorescence. Alternatively, purified particles were dissolved in cyanide solution, and the concentration of DNA was determined as described above. In the case of thin films, centrifugation was replaced by washing.

(23) Seeman, N. C. *Nature* **2003**, *421*, 427−431.
(24) Grabar, K. C.; Freeman, R. G.; Hommer, M. B.; Natan, M. J. *Anal. Chem.* **1995**, *67*, 735−743.
(25) *Practical Surface Analysis by Auger and X-ray Photoelectron Spectroscopy*; Briggs, D., Seah, M. P., Eds. Wiley: New York, 1983.

In the case of PNA−PNA hybridization, the tethered PNA was fluorescently labeled instead of the target sequence. Following purification, the hybridized nanoparticles were dissolved in cyanide solution as described above, the pH was adjusted to 7.3 with HCl, and the solution diluted in the 5 mM buffer prior the fluorescence being measured. The concentration of hybridized strands was determined by comparing the extent of fluorescence quenching to a control preparation in which 100% of the fluorescein-labeled strands were hybridized to their complements.

Characterization of Au Thin Films by XPS and Ellipsometry. XPS was performed using a Kratos Axis Ultra spectrometer with a monochromatic Al Kα source (15 kV, 10 mA) using 0.1 eV data spacing, a pass energy of 40 eV, and a takeoff angle of 0°. Ellipsometric measurements were made on a Sentech Instruments SE 400 ellipsometer equipped with a He−Ne laser (wavelength 632.8 nm), with a 70° angle of incidence from the surface normal.

PNA-Directed Nanocrystal Assembly. Assembly of PNA- and DNA-coated nanocrystals was directed by either PNA or DNA linker strands complementary to recognition sites on the immobilized strands. Assemblies using DNA linker strands were carried out either by adding the linker to a combined solution of the two modified nanoparticles or by prehybridizing the linker to one of the nanoparticles prior to combination. In the former case, 17 μL of 3 μM linker DNA was added to a solution consisting of 241 μL each of 6.2 nM modified nanoparticles in 5 mM PB containing 93 mM NaCl (103 mM Na^+). For prehybridization, a 10 nM solution of one modified nanoparticle was first incubated in 3 μM linker DNA in 5 mM PB + 90 mM NaCl (100 mM Na^+) for 12 h, and the hybridized nanoparticles were purified by centrifugation. Then, 6 nM solutions of the prehybridized and complementary nanoparticle in 5 mM PB + 90 mM NaCl were combined. For assemblies using a PNA linker strand, 241 μL of 6.2 nM solutions of each modified particle in 5 mM PB (10 mM Na^+) were combined, and 17 μL of 7.5 μM linker PNA was added. After at least 1 h at RT, the PNA linker systems were frozen in a dry ice/isopropyl alcohol bath for 1 h to facilitate assembly, thawed to RT, and allowed to continue assembly. The progress of the latter was followed in each case by spectrophotometry in each case by monitoring changes in the nanoparticle surface plasmon band. Assembly mixtures were agitated to disperse aggregates prior to the measurements.

Transmission Electron Microscopy. TEM micrographs of nanoparticle aggregates were obtained on a JEOL 100CX transmission electron microscope operating at 80 keV. Samples were prepared by depositing approximately 10 μL of the assembly solution (redispersed by agitation) onto Formvar carbon-coated grids and wicking away any excess solution. Grids were allowed to dry for at least 1 h prior to imaging.

Acknowledgment. This study was financially supported by NIH Grant GM26698. R.C. is an NIH postdoctoral fellow. XPS analysis was carried out using instrumentation in the MIT Center for Materials Science and Engineering. TEM micrographs were obtained at the Harvard Medical School Keck Microscopy Facility. We thank Prof. Scott R. Manalis for allowing the use of his ellipsometry and metal deposition equipment employed in this work.

Supporting Information Available: Details of PNA and DNA synthesis, XPS data characterizing PNA monolayers on thin films, and discussion of the mechanism of hybridization enhancement by mercaptosuccinic acid (PDF). This material is available free of charge via the Internet at http://pubs.acs.org.

JA035399G